HHS Public Access

Author manuscript

Adv Healthc Mater. Author manuscript; available in PMC 2022 March 01.

Published in final edited form as:

Adv Healthc Mater. 2021 March ; 10(5): e2000690. doi:10.1002/adhm.202000690.

Internally Responsive Nanomaterials for Activatable Multimodal Imaging of Cancer

Zachary T. Rosenkrans,
Department of Pharmaceutical Sciences, University of Wisconsin-Madison, Madison, WI 53705, USA

Carolina A. Ferreira,
Department of Radiology and Department of Medical Physics, University of Wisconsin-Madison Madison WI 53705, USA

Dalong Ni,
Department of Radiology and Department of Medical Physics, University of Wisconsin-Madison Madison WI 53705, USA

Weibo Cai
Department of Pharmaceutical Sciences, University of Wisconsin-Madison, Madison, WI 53705, USA; Department of Radiology and Department of Medical Physics, University of Wisconsin-Madison Madison WI 53705, USA

Abstract

Advances in technology and nanomedicine have led to the development of nanoparticles that can be activated for multimodal imaging of cancer, where a stimulus induces a material modification that enhances image contrast. Multimodal imaging using nanomaterials with this capability can further combine the advantages and overcome the limitations of any single imaging modality. When designed with stimuli-responsive abilities, the target-to-background ratio of multimodal imaging nanoprobes increases because specific molecular targets in the tumor enhance the signal. Several aspects of the tumor microenvironment can be exploited as an internal stimulus response for multimodal imaging applications, such as the pH gradient, redox processes, overproduction of various enzymes, or combinations of these. In this review, design strategies are discussed and an overview of the recent developments of internally responsive multimodal nanomaterials is provided. Properly implementing this approach improves noninvasive cancer diagnosis and staging as well as provides a method to monitor drug delivery and treatment response.

Graphical Abstract

wcai@uwhealth.org; dni2@wisc.edu.

Conflict of Interest
The authors declare no conflict of interest.

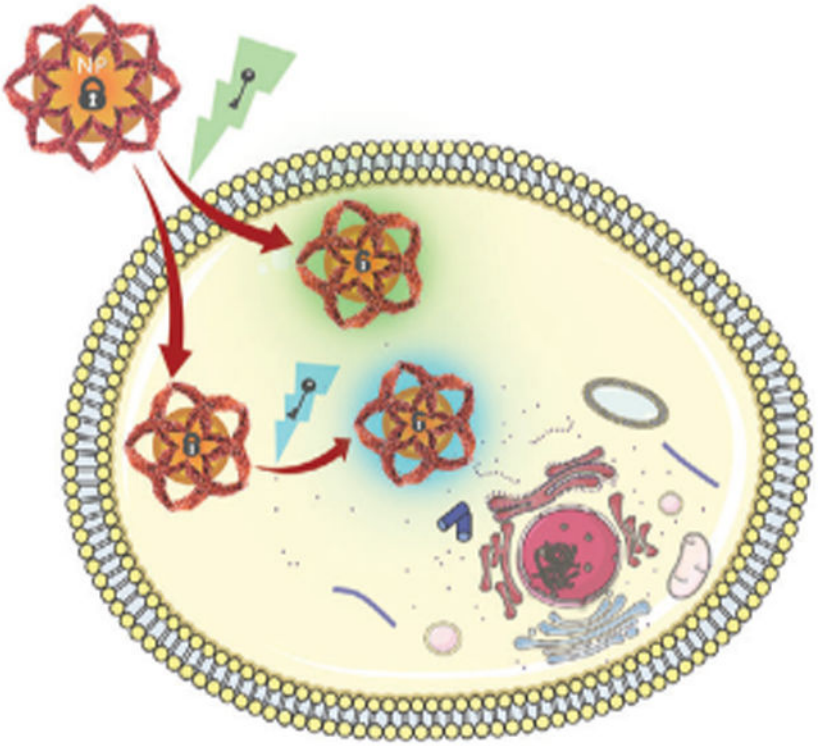

Internally responsive nanomaterials that respond to low pH, redox gradients, overexpressed enzymes, or combinations for activatable multimodal imaging is a significant advancement in the nanomedicine field in recent years. Designs using this strategy maximize disease-to-background signals while simultaneously providing anatomical and biological information for improved disease diagnosis, treatment monitoring, or image-guided surgical resection of diseased tissue.

Keywords

bioresponsive; internally responsive; multimodal imaging; nanomedicine

1. Introduction

The biomedical technology for noninvasive cancer imaging applications has matured over time. The toolbox available in pre-clinical or clinical settings includes optical imaging, photoacoustic (PA) imaging, positron emission tomography (PET), single photon emission computed tomography (SPECT), magnetic resonance imaging (MRI), X-ray computed tomography (CT), or others to inform cancer diagnosis and monitor treatment.[1] These modalities are often classified as either molecular or anatomic imaging, depending on the type of information they provide.[2] Traditionally, molecular imaging techniques (PET, SPECT, and optical) are used to visualize biological processes at the cellular and molecular levels. In contrast, structural imaging techniques (CT, MRI, and PA) provide anatomical information.[3] The nature of these various imaging modalities, in part, introduces advantages and disadvantages for each (Figure 1). Proper implementation of these modalities provides valuable information for cancer diagnosis and guide treatment regimens.

Multimodal imaging is a powerful strategy that combines two or more imaging modalities to provide complementary and reliable information about disease sites.[4] The coalescence of these conventional imaging techniques is done to combine their strengths and limit deficiencies.[5] While a functional and structural imaging technique is not always integrated, multimodal imaging often integrates anatomical information that provides high spatial resolution and biological information that offers high sensitivity at the molecular level and temporal resolution. In this manner, novel information about the diseased site is available for proper diagnosis and staging or treatment monitoring.

The nanotechnology field has been extensively explored in recent decades.[6] Nanomaterials are generally designed to alter pharmacokinetic properties to permit controlled delivery. With the progression of biomedical research, studies have found that nanoparticles (NPs) have ideal characteristics for multimodal imaging applications.[7] First, the size, surface charge, and shape can be modified to improve circulation and enhance delivery to disease sites. Second, NPs have been engineered with various surface chemistries that permit a wide array and multiple imaging agents to be incorporated into the design. Finally, the large surface area or internal volumes enable numerous imaging agents to be delivered to the disease site for enhanced signal.

Researchers have found that the signal-to-background of nanoprobes in imaging applications is improved by designing them to be stimuli-responsive.[8] Activatable imaging agents are those that are “turned on” for intensified image contrast once modified by a stimulus, which typically occurs by degradation or cleavage of the nanocomplex. The stimuli for signal activation may be internal or external to the imaging subject. Internally responsive nanomaterials exploit the microenvironment in disease sites for improved imaging and therapy applications.[9] Nanomaterials have been designed to be responsive to numerous internal stimuli that exist in the tumor microenvironment (TME), such as pH, redox processes, or through interactions with enzymes and proteins.[10] Another advantage of internally responsive nanosystems is that the distinction of whether an imaging modality is classified as a molecular or structural begins to blur. For example, a pH-responsive MRI nanomaterial contrast agent provides context of the diseased-tissue anatomy but also provides physiological information.[11] Importantly, this can provide precise information for imaging biological processes. While not the focus of this article, the stimuli for nanomaterial activation might alternatively be exogenous, such as light, magnetic fields, ultrasound, radiation, etc. For readers interested in imaging and therapeutic applications with nanomaterials that are responsive to exogenous stimuli, we refer them elsewhere.[12]

The focus of our review is internally responsive activatable multimodal imaging nanoplatforms, emphasizing the strategies required to engineer these systems. These nanoprobes exploit aspects of the TME, such as slightly more acidic pH, high levels of hydrogen peroxide (H_2O_2) and glutathione (GSH), overexpression of enzymes, or various combinations of these. Specific and rapid imaging of biological processes using multimodal systems that are activated in response to interaction with a specific molecular target is a powerful tool. While providing complementary anatomic, pathological, and molecular information of the tumor, activatable multimodal imaging nanoprobes hold immense potential for informed, personalized medicine. These nanoplatforms may support the

accurate diagnosis, guide therapeutic inventions, monitor drug distribution and therapeutic response, and facilitate image-guided surgery. In contrast, imaging strategies that are "always on" often have difficulty distinguishing anatomical features or biological events due to poor target-to-background signal ratios. In the following sections, we briefly describe the aspect of the TME that are used as stimuli for activatable multimodal imaging nanoprobes. We then outline applications reported categorized by the stimuli employed, where an internal stimulus activates at least one of the imaging modalities.

2. Tumor Microenvironment

Over the years, significant research efforts have elucidated the unique composition of the TME. These commonalities are valuable since they would exist in theory in all tumor types. The TME is complex, composed of vasculature, cancer-associated fibroblasts, immune cells, tumor-associated endothelial cells, and extracellular matrix.[13] Since a thorough discussion of the TME is beyond the scope of this review, we refer readers to other excellent reviews.[14] Together, the components of the TME are responsible for the unique properties that can be exploited for stimuli response.

The aspects of the TME frequently exploited when developing internally stimuli-responsive multimodal imaging agents are pH gradients, redox potential, and protein expression levels. The uncontrolled cellular growth in tumors generates high glycolytic rates under aerobic and anaerobic conditions in combination with poor lymphatic drainage generates excess lactic acid that leads to a TME is often slightly more acidic compared to physiological pH.[15] While the pH difference is usually small (≈1), careful material design can exploit this and result in drastic changes to imaging properties.[16] The reductive environment in tumors stems from elevated levels of reactive oxygen species (ROS) as well as high levels of GSH relative to NADPH.[17] This difference in redox potential leads to GSH levels that are approximately four times higher in tumor tissue compared to normal tissue.[18] As such, this is a stimulus-specific to cancer cells that can be used for activation. Another valuable stimulus is enzymes, which are essential regulators of cellular processes. The expression of enzymes, such as proteases, is often altered in various disease states such as cancer.[19] The increased enzyme levels enable imaging activation by enzymatic conversion of the nanomaterial. While each of these stimuli are valuable to achieve activatable imaging on their own, it is possible to design an intelligent nanosystem that can respond to a combination of them. Exploiting these elements of the TME for multimodal imaging applications can provide a comprehensive overview of the anatomical, physiological, and molecular information of the tumor using a single imaging nanoplatform.

3. Internal Targets for Nanomaterial Activation

In the following sections, we will discuss biomedical applications of nanomaterials that exploit variations in pH, redox potential, enzyme expression, or a combination of these to achieve activatable multi-modal imaging.

3.1. pH

The slight acidity of the TME compared to healthy tissue and blood has been widely used to design activatable imaging and therapeutic nanosystems.[20] Several strategies have been proposed to endow nanoprobes with pH-responsive multimodal imaging properties. Typically, pH-activated imaging is achieved by designing nanomaterials that are degraded, including moieties that are altered by protonation of amine groups, or incorporating segments that are cleaved or released under slightly acidic conditions. Inorganic, organic, and hybrid nanomaterials have all been used in this strategy and often dictate the mode of activation. Imaging probes with this functionality enable the visualization of pH variations during cancer diagnosis and throughout treatment regimens. pH visualization provides invaluable information about changes in metabolism and may inform clinicians of treatment efficacy by reflecting changes in the glycolytic rates.

3.1.1. pH Activation by Material Degradation—Manganese (Mn^{2+})-based nanomaterials are often used to design nanoprobes that are activated by acid-mediated degradation, which are usually formed using nanosheets or by coating materials. Manganese (II) oxide (MnO) NPs are often used as longitudinal relaxation time (T_1)-weighted MR contrast agents because they decompose and release paramagnetic Mn^{2+} under weakly acid conditions. Gao and co-workers prepared small-sized octapod-shaped hollow porous MnO (HPMO) NPs for activatable MR and FL imaging.[21] This nanosystem could also be loaded with various cargo (Cargo@HPMO), such as camptothecin (CPT) or Rhodamine 123 (Rh123), for additional FL functionality. When HPMO was degraded in an acidic environment, the Mn^{2+} produced enhanced the T_1-weighted contrast. CPT and Rh123 were simultaneously released and increased the FL intensity because of the decreased aggregation-caused quenching (ACQ) effect. In a theranostic approach, this nanosystem could be loaded with therapeutic cargo to enable drug delivery visualization as it is released in the tumor. The delivery and endocytosis of MnO-based nanomaterials can be improved by adding targeting ligands. This enhances the nanomaterial design when the intracellular pH (≈5.5) is required for activation compared to the extracellular pH (≈6.5). Wang and colleagues utilized this strategy when they encapsulated MnO NPs and coumarin-545T (C545T) inside a poly(ethylene oxide)-based silica nanocapsules (MC-NCs) that were decorated with folate receptor targeting folic acid (FA).[22] Under normal physiological conditions, the FL intensity of C545T was quenched by the MnO NPs due to ACQ. However, acidic conditions released Mn^{2+}, which decreased the quenching of the C545T FL and enhanced MR contrast. A significant limitation of MnO-based nanoprobes is that they frequently experience rapid Mn^{2+} release in acidic conditions, which prevents prolonged T_1-contrast. To overcome this problem, Liu et al. synthesized porous gold nanocluster decorated MnO nanocomposites (MnO@Au NCs).[23] The Au NCs decorated on the surface of the MnO NPs enabled excellent qw and broad near-infrared (NIR) absorption. Due to the porous nature of the Au NCs layer, the MnO core was still accessible to aqueous environments. However, this unique structure increased the stability at normal physiological pH and slowed the release of Mn^{2+} for delayed T_1-contrast under acidic conditions.

Calcium carbonate ($CaCO_3$) is another inorganic nanomaterial that can be used to design nanosystems in the acid milieu of tumors. Dong et al. used $CaCO_3$ as the foundation to

develop organic-inorganic hybrid NPs that could be activated for enhanced T_1-MR contrast in response to the low pH of the tumor microenvironment.[24,25] The $CaCO_3$ NPs were prepared using a gas diffusion reaction under vacuum where ammonia bicarbonate (NH_4HCO_3) was used to precipitate Ca^{2+} ions in an ethanol solution, resulting in $CaCO_3$ formation under the alkaline conditions. In an initial study, chlorine e6 (Ce6) and $MnCl_2$ were loaded into the NPs by dissolving them in the ethanol solution and then PEGylated under sonication (Ce6(Mn)@$CaCO_3$-PEG). The Ce6(Mn)@$CaCO_3$-PEG NPs were sensitive to pH due to the $CaCO_3$ that was used as the backbone. Under increasingly acidic conditions, the Ce6(Mn)@$CaCO_3$-PEG NPs were degraded and released loaded Ce6(Mn) (Figure 2a). As a result, the T_1-contrast for MR imaging was enhanced due to the increased coordination of water molecules with unpaired Mn electrons. This effect was also observed using in vivo murine tumor models that showed a high T_1 signal in MR imaging studies (Figure 2b). Simultaneously, FL imaging was possible because of the excitation and emission properties of Ce6, which characterized the biodistribution of the nanomaterial on a systemic level. In another study, the synthesis was slightly altered by adding dopamine in the ethanol solution, which accelerated $CaCO_3$ growth and was oxidized to form polydopamine (PDA), resulting in the formation of $CaCO_3$-PDA-PEG hollow composite NPs. The incorporation of PDA in this design made it possible to chelate various metal ions (e.g., Fe^{3+}, Zn^{2+}, Mn^{2+}, or Co^{2+}) for multiple imaging modalities and provided absorbance in the NIR region for PA imaging. In vivo imaging of this nanosystem after chelating Mn^{2+} provided both structural and functional information regarding the tumor using MR and PA imaging (Figure 2b). As shown in Figure 2c, pH-responsive FL imaging occurred as a result of the breakdown of the NP structure in a slightly acidic environment that released Ce6 and decreased PDA-mediated FL quenching.

3.1.2. pH Activation by Amine Protonation—Incorporating proton-sensitive amine groups into nanomaterials is an effective method to control image contrast, which is often accomplished using pH-sensitive polymers to prepare either organic or hybrid nanoparticles. A significant advantage is that highly specific activation can be achieved based on the pKa of the component for selective activation in the extracellular or lysosomal pH. Chen and co-workers developed PEGylated-gadolinium metallofullerene-polypyrrole (PEG-GMF-PPy) NPs.[26] The pH-sensitive polymer (PEG-PC7A), which was conjugated to the surface of the PPy NPs, underwent a hydrophobic-to-hydrophilic conversion after acid-activation (transition pH is ≈6.9) that increased the accessibility of water molecules to the GMF layer to enhance T_1weighted contrast. Since PPy NPs also absorbed NIR light strongly, PA imaging could also be used to visualize the tumor. Imaging sensitivity can be further improved by using nanoprobe designs with bimodal activation capabilities. A dual PA and FL imaging activatable nanosystem based on pH-responsive perylenediimide (PPDI) NPs was synthesized by Yin and colleagues.[27] Their strategy incorporated a pH-sensitive piperazine ring and perylenediimides that self-assembled into NPs. In acidic environments, FL and PA signal increased after the piperazine ring was protonated. Signal enhancement was attributed to the resulting limitation of PET from the methyl-substituted nitrogen atoms to the perylene chromophore. However, a gradual increase in the FL and PA intensity was observed as the pH decreased from 7 to 5, which may increase the tumor-to-background ratio compared to nanomaterials that have sharp signal enhancements. A much more specific

pH activation was reported by Wang et al. when they prepared photosensitizer-conjugated acid-switchable micelles for acid-activatable FL and MR imaging.[28] Core–shell micelles were self-assembled from a Gd-chelated Ce6 conjugated to the ultra-pH-responsive diblock copolymer poly(ethylene glycol)-*block*-poly(diisopropanol amino ethyl methacrylate cohydroxyl methacrylate (PDPA) complex. In moderately low pH conditions (≤6.2), the tertiary amines on PDPA were protonated and induced dissociation of the micelles. Strong FL intensity and T_1contrast were generated by limiting the fluorescence resonance energy transfer effect/photoinduced electron transfer from the nitrogen atom of PDPA and increased accessibility of water molecules to Gd^{3+}, respectively.

Hybrid organic–inorganic nanomaterials can also be used for activatable multimodal imaging mediated by protonation of amines under acidic conditions. pH-sensitive magnetic nanogrenades (PMNs) were prepared by Hyeon and colleagues for ultrasensitive bimodal imaging of tumors.[29] The PMNs were composed of extremely small-sized iron oxide nanoparticles (ES-IONs) self-assembled with two ligands, both containing Ce6 and imidazole for FL capacity and pH sensitivity, respectively (Figure 3a). Additionally, one ligand was conjugated with catechol groups that have a high affinity for ESIONs, and the other was used to produce a critical phase transition in response to acidic conditions. As shown in Figure 3b, the pH decreased, imidazole in the PMNs is protonated and causes the platform to swell. Further decreases in pH cause the PMNs to disassemble as a result of diminished hydrophobic interactions in the core. The authors demonstrated that when the pH was reduced from 7.5 to 5.5, PMNs had a longitudinal relaxivity (r_1) increase and transverse relaxivity (r_2) decrease, both of which are required for iron oxide NPs to be used as T_1weighted contrast agents (Figure 3c). These effects resulted from increased and sustained coordination of water molecules with the ESIONs. Similarly, fluorescence intensity from PMNs was partially quenched at pH 7.4 due to fluorescence resonance energy transfer caused by aggregation of the fluorophores but increased at a pH less than 6 (Figure 3d). Interestingly, both effects were reversible and enabled pH mapping of tumors in real-time. PMNs were then injected intravenously into ultrasmall HCT116 tumor-bearing mice (≈3 mm) to determine whether these effects would be observed in vivo. As shown in Figure 3e,f, FL and MR imaging studies delineated the tumor and facilitated the monitoring of the various organ uptake. These results indicated that PMNs could be used to effectively diagnosis tumors and provide valuable information regarding the pH of the tumor microenvironment.

3.1.3. pH Activation by Incorporating an Acid Liable Group—The last commonly used strategy for pH-activatable multimodal imaging nanoprobes involves incorporating an acid liable group.[30] This method of activation also benefits from the high specificity of the pKa of the functional group used for acid-mediated ligation. The Yang group used this approach when they prepared a pH-activatable TAT peptide functionalized on the surface polymeric NPs loaded with Ce6 and Gd^{3+} (^{DA}TAT-NPs), where 2,3-dimethylmaleic anhydride (DA) was conjugated to the TAT via lysine residues.[31] In a slightly acid environment, the amide bond formed in ^{DA}TAT-NPs would degrade to the reactive TAT peptide for active targeting to increase FL and MR signal but did not occur when succinic anhydride was used as a control (^{SA}TAT-NPs).

Studies have shown that acid liable groups can also be incorporated into hybrid organic–inorganic nanomaterials for activatable multimodal imaging. Zhu and co-workers developed an acid-cleaved nanoprobe for activatable FL and CT imaging. Their nanosystem was composed of gold nanoparticles (GNPs) conjugated via a ketal linker to a NIR fluorophore (Cy5.5) and decorated with FA to enable active targeting of the folate receptor (GNPs-CKL-FA).[32] The GNPs core enhanced CT contrast and also quenched FL from Cy5.5 under physiological pH. Hydrolysis of the ketal linker occurred under pH conditions comparable to the TME (6.5), which dramatically enhanced the FL signal from GNPs-CKL-FA. Intravenous injection of GNPs-CKL-FA was able to clearly delineate subcutaneous HeLa tumors in mice. More detailed quantification of pH at the cellular levels was achieved by Yu et al. when they prepared dual-modal smart nanovehicles for pH-sensing.[33] Gold nanoparticles were synthesized for the core of the material, which was decorated with cyclic argininegylcine-aspartic acid peptide (cRGD) to target $\alpha_v\beta_3$ expressed on tumors and a mitochondria targeting group (Mito-S). Dual pH-sensitivity was endowed by incorporating rhodamine (Rh-S) and fluorescein (Flu-S) derivatives, where the FL intensity of both was modulated by ring-opening of the spiro-ring unit under acidic or basic conditions, respectively. Finally, a Gd^{3+} containing moiety (Gd-S) was embedded on the GNPs surface for T_1-weighted MR imaging. The multifunctionality of this nanoprobe (D-Au@Gd&RGD) enabled sensitive detection of pH because the two FL compounds had different emission wavelengths. In vivo MR and FL imaging of D-Au@Gd&RGD in U87 tumor-bearing mice successfully visualized the tumor, which was compared to a nontargeted control.

The Mn^{2+} used in many of the previously mentioned bioresponsive platforms introduces toxicity concerns. Properly designing nanomaterials that are activated by cleavage at low pH has been used to overcome this problem. Gao and colleagues developed an activatable, multimodal imaging core–shell nanoprobe composed of upconversion luminescence nanoparticles (UC-NPs) as the core and an iron (Fe^{3+})/gallic acid (GA) complex as the shell (UCNP@GA-Fe^{III}).[34] The nanomaterials were prepared by synthesizing $NaGdF_4$ nanocrystals doped with Yb, Tm, and Ca, which were then PEGylated by ligand displacement and conjugated with GA that could complex Fe^{III}. While pH-responsive T_1-weighted contrast is typically arduous to achieve using Fe^{3+} because of the stability of Fe-O-Fe under slightly acidic conditions, it was possible in this case because the Fe^{III} complex was unsaturated by coordination with HO^- and H_2O. Under acidic conditions, phenylic hydroxyls were protonated, breaking the superexchange coupling, and released Fe^{III} from GA (Figure 4a). This careful design resulted in a molar relaxivity increase from 3.2 mM^{-1} s^{-1} at pH 7 to 9.2 mM^{-1} s^{-1} at pH 4 for UCNP@Ga-Fe^{III}. Since the Ga-Fe^{III} coating absorbed multiple emissions from the UCNPs, it was demonstrated the ratio of two emissions (I_{470}/I_{802}) could be used to quantitatively monitor the release of Fe^{3+} in response to pH (Figure 4b,c). In vivo MR imaging of tumors demonstrated sustained T_1-contrast enhancement up to 24 h, which was attributed to the sustained release of Fe^{3+} (Figure 4d,e). At equivalent doses, upconversion luminescence imaging studies correlated the T_1-contrast enhancement with Fe^{3+} release by relating emission at 475 and 802 nm. This novel design employs sensitive imaging modalities to monitor the release of Fe^{3+}. Importantly, the Fe^{3+} in this system eliminates many of the toxicity concerns of Mn^{2+} used in many other activatable multimodal nanoplatforms.

3.2. Redox Potential

The reductive TME possesses another unique stimulus that can be used to design activatable multimodal imaging nanosystems. The two aspects of tumors that are often exploited in tumors are the elevated levels of GSH and ROS. In this section, we discuss examples of strategies that have been utilized for both targets.

3.2.1. Biothiols, Including GSH—The most representative biothiol is GSH, which is a three amino acid peptide that has the primary role of maintaining the balance of oxidative stress in cells.[35] The antioxidant properties of GSH arise from the equilibrium between its reduced and oxidized forms. Elevated levels of GSH have been observed in diverse cancer types, which often increases the resistance of tumor tissue to chemotherapies.[36] The majority of biological GSH resides in the cytosol of cells, where concentrations can be as high 10×10^{-3} M as opposed to the extracellular environment.[37] Unsurprisingly, GSH has arisen as an attractive stimulus to activate multimodal imaging nanoprobes. GSH sensitivity is typically accomplished by including bonds that can be reduced by GSH, such as disulfide bonds, or by using materials that can be degraded by GSH.

Many GSH-responsive nanomaterials are designed by exploiting moieties that are easily reduced, such as disulfide bonds or sulfonyl groups.[38] Santra and colleagues utilized this strategy to develop an activatable multimodal imaging nanosystem.[39] Dihydrolipoic acid-modified superparamagnetic iron oxide nanoparticles (IONPs) were used as the core and conjugated with FA- and STAT3 inhibitor-functionalized CdS:Mn/ZnS quantum dots (QDs) (MMCNP). After GSH-mediated reduction, the QDs were released via disulfide bond cleavage from the IONPs, which eliminated the FL quenching. Structural information could also be obtained using the MR-contrast provided by the IONPs core. Another interesting example was reported by Hu et al. when they prepared human serum albumin nanoassemblies (HSA NAs).[40] GSH-sensitivity resulted from the facile method used to make the HSA NAs, where GSH was used to obtain free sulfhydryl groups that were cross-linked and then loaded with Ce6 via hydrophobic interactions and later chelated with Mn^{2+} (HSA-Ce6-Mn^{2+} NAs). Endocytosis of HSA-Ce6-Mn^{2+} NAs into the GSH-rich cytoplasm of cancer cells cleaved the disulfide bonds, breaking the NAs, and triggering FL signal recovery as the Ce6 was released. Simultaneous MR and PA imaging also visualized tumors in murine models and enhanced the information obtained from HSA-Ce6-Mn^{2+} NAs.

In 2016, Zheng et al. synthesized self-assembled NPs that were activated in a GSH-rich environment for trimodal responsive imaging.[41] Their nanomaterial was assembled from π;–π interactions of a probe containing a Gd^{3+} chelate, ^{19}F moiety, and a disulfide-capped amino-oxyluciferin fluorophore (Figure 5a). The principle for the nanomaterial was the paramagnetic relaxation enhancement (PRE) effect, which involves an increase in nuclear relation rates from magnetic dipolar interactions between a nucleus and unpaired paramagnetic electrons.[42] Due to the proximity of the Gd^{3+} chelate and ^{19}F moiety and quenching from hydrophobic interactions, the ^{19}F signal was absent under physiological conditions. However, T_1-weighted ^1H-MR contrast from the Gd^{3+} chelate would be high. When delivered to the reductive TME containing elevated biothiols, such as GSH, the ^{19}F compound capped by a disulfide bond to the fluorophore was cleaved. Disulfide cleavage

also initiated spontaneous disassembly of the nanoparticle by removing the linker to the caging group. As shown in Figure 5b, disassembly induced by GSH resulted in a 70-fold increase in fluorescence intensity, 30-fold amplification of ^{19}F MRS signal, and 68% decreased r_1 relaxivity (0.5 T). Subcutaneous injection of Matrigel containing the self-assembled NPs with 10×10^{-3} M GSH resulted in drastically increased FL intensity (Ex/Em = 420/540 nm) and decreased T_1-weighted MR signal compared to when GSH was omitted (Figure 5c,d). Additionally, the self-assembled NPs with (**1**) or without (**1-ctrl**) a reducible disulfide bond were compared by intravenous injection into HeLa tumor-bearing mice. Owing to reduction from biothiols, T_1-weighted MR images demonstrated that NPs **1** had reduced signal intensity in the tumors compared to NPs **1-ctrl** as rapidly as the 1 h time point. This promising platform could be slightly modified to include linkers that are cleaved in response to other stimuli for activatable multimodal imaging of different biological processes.

Researchers have also found that GSH can induce the degradation of nanomaterials, which can be exploited for the activatable multimodal imaging applications. Several reports of this strategy are based on manganese dioxide (MnO_2) nanosheets, which decompose after reduction by GSH. In the native MnO_2 state, Mn atoms do not influence proton relativity because they are shielded from the aqueous environment by oxygen atoms. The degradation of MnO_2 nanosheets releases large amounts of Mn^{2+}, which dramatically enhances T_1-weighted MR contrast. The generated contrast from MnO_2 is significantly enhanced compared to other materials, such as commercially available Gd-based CAs.[43] Multifunctionality with MnO_2 nanosheets is easily accomplished by absorbing compounds onto their surface. Incorporating a FL moiety, which is quenched by MnO_2, is an example of a design strategy to provide activatable FL imaging as it is released from the nanosheets and no longer quenched.[44]

The sensitivity and specificity of the GSH-induced degradation strategy can be enhanced by adding a targeting feature. Tan and colleagues reported a dual activatable FL/MR imaging platform based on reducible MnO_2 nanosheets.[45] Ultrasonication of bulk MnO_2 synthesized from $MnCl_2$ was used to prepare MnO_2 nanosheets. After Cy5-labeling and adding an additional 19 base at the 5′ terminus, a 60-base sgc8 aptamer targeting protein tyrosine kinase 7 (PTK7) was absorbed onto MnO_2 nanosheets (≈2.9 pmol μg^{-1} of MnO_2 nanosheet). Prior to interacting with cells, the FL intensity from Cy5 was quenched by the MnO_2 nanosheets, and MR contrast was weak due to a low Mn^{2+} concentration. Endocytosis of the MnO_2 nanosheet-aptamer nanoprobe was enhanced after binding to PTK7-positive cells. Subsequently, the reduction of the nanoprobe by intracellular GSH led to a release of the Cy5-labeled aptamer and fluorescent activation and dissolution of the nanosheet into Mn^{2+} for MR contrast. The authors confirmed this by comparing the FL intensity of flow cytometry with PTK7-positive cells (CCRF-CEM) and PTK7-negative cells (Ramos). Additionally, adding GSH to the MnO_2 nanosheet-aptamer nanoprobe resulted in r_1 and r_2 enhancements of 48- and 120-fold, respectively. In subsequent studies, the Fan group modified the MnO_2 nanosheets with using Ce6 and Ce6-labeled DNAzymes for activatable FL/MR imaging and were also applied for photodynamic therapy and gene silencing.[46] The

mechanism in these similarly required GSH-mediated reduction of the MnO_2 nanosheets for FL/MR activation and therapy.

3.2.2. Reactive Oxygen Species—Abnormal GSH expression disrupts related cellular processes that result in high levels of oxidative stress.[47] The associated elevated levels of ROS in cancer cells can also be used as a stimulus for activatable imaging. Excess ROS have been found in many cancer types, with examples including hydrogen peroxide (H_2O_2), superoxide anion ($O_2^{\bullet -}$), hydroxyl radicals ($^{\bullet}OH$), among others.[48] Under normal homeostasis, low ROS levels are carefully maintained by cells using various mechanisms. However, levels of ROS in almost all cancers are aberrantly high due to increased metabolic activity, mitochondrial dysfunction, and other oncogenic functions.[49] With proper design, ROS-activated multimodal imaging nanoprobes are very promising.

MnO_2-based nanomaterials also have redox-sensitive properties that can be exploited for activatable multimodal imaging applications.[50] Degradation of MnO_2 nanosheets can occur via the following reaction, which is catalyzed by MnO_2: $2H_2O_2 \rightarrow 2H_2O + O_2$. As an example, Peng et al. prepared biodegradable Prussian blue (PB)/MnO_2 hybrid nanocrystals (PBMn-52) via the reduction of potassium permanganate (Figure 6a,b).[51] The MnO_2 incorporated into the PB framework, which contains both Fe(II) and Fe(III), decreased the r_2 while also increasing the r_1. Interestingly, when PBMn-52 was incubated with H_2O_2, both the r_1 and r_2 increased from 4.9 and 15.2 mM^{-1} s^{-1} to 32.4 and 28.3 mM^{-1} s^{-1}, respectively. As demonstrated in Figure 6c,d, PA and MR imaging studies demonstrated that PBMn-52 was an effective contrast agent. While this is an important aspect of MnO_2-based NPs, they are often shown to have enhanced signal contrast combined with other stimuli such as low pH or increased GSH levels. As such, they are discussed in further detail in the multistimuli-responsive section.

Other ROS-activated nanoprobes can be designed using ROS-sensitive polymers. Bouché et al. prepared an H_2O_2-activated CT and PA imaging.[52] In their design, gold nanoparticles (AuNPs) were loaded into hybrid polyphosphazene derived polymer nanogels formed through ionic interactions (PPB NPs). The sensitivity of this nanoprobe to ROS stemmed from the nanogel coating composed of poly[di(carboxylatophenoxy)phosphazene] (PCPP) and the arylboronate polyphosphazene derivative (PPB). PPB degrades in response to ROS through the formation of an unstable glycine-functionalized polyphosphazene that self-catalyzes additional backbone degradation into phosphates and ammonia. At the same time, PCPP biodegrades into products that are nontoxic and have a neutral pH. Erosion of the nanogel coating by H_2O_2 released the AuNPs payload, which reduced the PA signal intensity by decreasing the collective plasmon resonance effect. In comparison, the CT contrast was unaffected after PPD NPs were incubated with H_2O_2. The PPB NP nanosystem was then evaluated in vitro using a macrophage cell line (RAW264.7) incubated with and without lipopolysaccharide and interferon-γ. Decreased PA signal but high CT contrast were observed for the inflamed macrophages incubated with PPB NP compared to controls. In comparison, similar NPs without the PPB moiety had a PA signal independent of ROS and were unable to differentiate ROS levels in the RAW264.7 cell line. While this design may provide a ratiometric method to differentiate ROS levels using PA and CT imaging, the

negative PA signal enhancement may complicate in vivo imaging with this nanosystem, which was not performed in this study.

3.3. Enzymes

Enzymes are proteins that act to accelerate chemical reactions by lowering the catalytic energy barrier in biological systems. In many cancer types, various genes are upregulated, leading to overexpression of enzymes.[53] Nanoprobes designed to activate selectively in response to the increased enzymatic catalysis can lead to a dramatic signal enhancement for disease diagnosis. In the following sections, we discuss enzyme-activated multimodal imaging nanosystems classified by the enzyme type used for activation.

3.3.1. Matrix Metalloproteinases (MMPs)—Matrix metalloproteinases include 26 calcium-dependent endopeptidases with functionality traditionally ascribed to degrading the extracellular matrix and are upregulated at all cancer stages.[54] Typically, MMP-activated multimodal imaging probes are designed by incorporating an MMP-cleavable peptide.[55] After enzymatic catalysis, the nanoprobe is turned on from a quenched to an active state. Here, we discuss multimodal imaging applications that involve MMP activation.

Gelatinases are a subtype of MMPs, which include MMP-2 and MMP-9, that have been extensively studied and implicated in angiogenesis and tumor growth.[56] The Tsieng group first reported gelatinase-activated bimodal imaging nanoplatform, composed of a functionalized dendrimer.[57] Cha et al. prepared an IONP core-silica shell NPs that were decorated with the same MMP substrate (GPLGVRG) (PCM-CS).[58] The FL signal from Cy5.5 was efficiently quenched by the IONP core, but increased by more than 97% after PCM-CS was activated by MMP-2. In vivo imaging after intravenous injection of PCM-CS was able to clearly visualize tumors using activatable FL imaging and transverse relaxation time (T_2)-weighted contrast provided by the IONP core.

An interesting application was reported by Shi et al., when they prepared a tumor-targeted and MMP-2 activatable nanoprobe (T-MAN) with activatable FL and MR bimodal imaging.[59] T-MAN was constructed by first synthesizing novel Gd/CuS nanodisks that were then encapsulated into micelles using DSPE-PEG2000 for improved solubility and biocompatibility. The micelles were then functionalized with an $\alpha_v\beta_3$ tumor-targeting group (cRGD-SH) and a Cy5.5- and QSY21-labeled MMP-2 cleavable peptide substrate ((QSY21)-GGPLGVRGK(Cy5.5)-SH). The presence of Gd^{3+} in the Gd/CuS nanodisks and geometric confinement in the micelles to further reduce molecular rotation endowed them with a high r_1 of 60 mM^{-1} s^{-1} (1 T). Before activation by MMP-2, the FL of Cy5.5 was quenched by the proximity of QSY21. Introducing MMP-2 to T-MAN, which cleaved the peptide at the GV site to release QSY21 from Cy5.5, enhanced the NIR FL intensity by ≈185-fold (Figure 7a). The enzymatic kinetic parameters for T-MAN and MMP-2 were found to be a K_m of 1.67×10^{-6} M and a k_{cat} of 0.12 s^{-1}, with a k_{cat}/K_m ratio 7.2×10^4 M^{-1} s^{-1}, which indicates efficient cleavage. The imaging abilities of T-MAN were evaluated after intravenous injection into mice bearing subcutaneous gastric cancer tumors (MKN45 cell line). As shown in Figure 7b, the FL intensity in the tumors gradually increased until a maximum was reached 12 h p.i. The tumors could be simultaneously delineated in T_1-

weighted MR images that provided anatomical context (Figure 7c). Importantly, the FL signal was significantly reduced when tumors were administered an MMP-2 inhibitor (SB-3CT), blocked with free RGD, or T-MAN without the $\alpha_v\beta_3$ targeting ligand (T-MAN-ctrl). The MR signal was also reduced when T-MAN was blocked with free RGD or when T-MAN-ctrl was administered but comparable to when the MMP-2 inhibitor was administered, suggesting MR contrast was independent of MMP-2 activity. Additional experiments found T-MAN similarly provided enhanced MR contrast 12 h p.i. and FL signal for surgical resection of tumors in an orthotopic gastric cancer model (Figure 7e,f).

Other studies have shown that NPs can be responsive to multiple MMPs. Kim and colleagues achieved this when they designed an activatable nanoprobe based on biocompatible glycol chitosan nanoparticles (CNPs). The CNPs provided activatable optical imaging and were also radiolabeled with Copper-64 (^{64}Cu, $t_{1/2}$ = 12.7 h) for PET imaging, which can monitor the biodistribution with unlimited tissue penetration and high sensitivity. Azide-functionalization of the CNPs was first carried out before additional modifications. Bioorthogonal click chemistry with the azide groups and dibenzylcyclooctyne (DBCO)-modified 1,4,7,10-tetraazacyclododecane-1,4,7-tris(t-butyl acetate)-10-acetic acid (DOTA; DOTA-Lys-PEG$_4$-DBCO), and an MMP-specific peptide with Cy5.5 for FL imaging and BHQ-3 as a quencher ((Cy5.5)-GPLGVRGK(BHQ3)GG-PEG4-DBCO) was used to conjugate them to CNPs. The MMP activity of the probe was then evaluated with MMP-2, 3, 7, 9, and 13, which found a significant FL signal enhancement with MMP-2, 9, and 13 and was inhibited with an MMP-2 inhibitor. The ^{64}Cu-labeled and activatable MMP-specific peptide-modified CNP (^{64}Cu-DOTA-AMP-CNPs) was then evaluated in multimodal imaging studies with A549 xenograft bearing mice. Near-infrared fluorescence (NIRF) imaging of ^{64}Cu-DOTA-AMP-CNPs delineated tumors as rapidly as 1 h p.i. and the signal in the tumor continued to increase until a plateau was reached at 6 h p.i. The specificity of the NIRF signal from MMPs was confirmed in another imaging study since an MMP inhibitor significantly decreased the FL intensity. A serial PET imaging study with ^{64}Cu-labeled CNPs successfully visualized the tumor, with a maximum tumor uptake of 6.2%ID g^{-1} at 24 h p.i. Ex vivo studies were able to confirm the NIRF and PET imaging in vivo findings. Due to the unique combination of a PET/optical imaging probe, the tumor-targeting efficiency could be quantified while simultaneously providing information on MMP activity that might aid treatment planning efforts.

While not used for cancer imaging, it is worth mentioning the MMP-activated nanoprobe developed by Gu and co-workers for imaging gelatinase activity in ischemic stroke.[60] They functionalized a dendrimer core with Cy5, Gd-DOTA, and an MMP-cleavable peptide. After inducing ischemic injury, excellent T_1-weighted MR contrast and enhanced FL intensity were observed in the damaged region.

3.3.2. Serine Proteases—Serine proteases, which account for more than one-third of all proteolytic enzymes and found in all kingdoms of cellular life,[61] have also been found to be valuable in activatable multimodal imaging applications. Strategies involving serine proteases are similar to other enzyme-activated nanosystems that require the use of an enzyme-specific peptide. However, some reports include activation by the degradation of the

NPs template. In this section, we highlight nanomaterials that can be activated by this enzyme type.

The Liang group reported an enzyme-activatable nanoplatform for dual-modal imaging.[62] Their core–satellite NPs were made of gelatin (Gel) NPs loaded with indocyanine green (ICG) and doxorubicin (DOX) that were then coated with PEGylated copper sulfide (CuS) NPs (ICG/DOX@Gel-CuS NMs), where FL from ICG was initially quenched. Incubating ICG/DOX@Gel-CuS NMs with trypsin resulted in the degradation of the gel matrix and recovery of the FL signal after releasing the CuS NPs from the surface. FL imaging with this "turn-on" ability in combination with PA imaging enabled real-time monitoring of drug release using this unique enzyme-activated nanosystem that did not require a specific, cleavable peptide sequence.

Fibroblast activation protein (FAP) is a serine protease commonly expressed on fibroblasts in tumor stroma and found in more than 90% of epithelial cancers.[63] Nie and co-workers designed a polydopamine-coated gold nanostars (GNS@PDA) nanoplatform (Figure 8a) using FAP as a stimulus for diagnostic imaging.[64] After synthesizing GNS@PDA, a Cy7-labeled FAP-cleavable peptide (Cy7-KTSGPNQC) was conjugated to the PDA shell using a Michael addition reaction (GNS@PDA-Cy7). PDA, which can chelate a vast array of metal ions, was complexed with Fe^{3+} ions for enhanced T_1-weighted MR contrast, while the GNS provided CT and PA imaging contrast and served as a NIRF quencher. Enzyme kinetic studies confirmed the reactivity of GNS@PDA-Cy7 with FAP, where kinetic constants were calculated to be 24.6×10^{-6} M and 12.1 min^{-1} for K_m and k_{cat}, respectively ($k_{cat}/K_m = 4.9 \times 10^5$ M^{-1} min^{-1}). FAP (0.5 μg mL^{-1}) mediated cleavage of GNS@PDA-Cy7 resulted in a 27-fold FL intensity enhancement within 6 h, which was initially quenched due to nanometal surface energy transfer from Cy7 and GNS in the nanomaterials. NIRF imaging after intravenous injection of GNS@PDA-Cy7 visualized activation of the nanoplatform in response to FAP, which reached a maximum signal enhancement 6 h p.i. (Figure 8b). As shown in Figure 8c,d, CT, PA, and MR imaging to elucidate tumor architectural information were simultaneously possible due to the gold, PDA, and Fe^{3+}, respectively, contained in the GNS@PDA-Cy7. This diagnostic nanosystem and future developments have immense clinical significance since high FAP expression is often associated with tumor malignancy and poor prognosis.[65]

Thrombin is a critical enzyme involved in thrombosis and has been found to influence tumor angiogenesis.[66] Kwon et al. prepared a thrombin-activatable fluorescent peptide (TAP) incorporated silica-coated gold nanoparticles (TAP-SiO_2@AuNPs).[67] They found that thrombin-mediated cleavage enhanced FL intensity by releasing Cy5.5, which was initially quenched by the AuNPs core that also provided CT contrast. Using a murine carotid thrombus model, they found that TAP-SiO2@AuNPs provided localized FL and CT signals to discriminate the thrombotic lesion.

3.3.3. Caspase—Apoptosis is a programmed cell death pathway that frequently occurs when DNA damage is irrepairable, maintaining the balance of dysfunctional and normal cells.[68] A central component of this specialized cellular pathway is a family of cysteine proteases called caspases.[69] Caspases are proenzymes that are activated during apoptosis

and function as both initiators and effectors to initiate cell disassembly in response to proapoptotic signals.[70] Research has found that caspase-3 and caspase-7 are primarily responsible for inducing apoptosis, which is the basis for most anticancer therapies.[71] As such, imaging techniques that visualize caspase activation, primarily caspase-3/7, would be immensely valuable for monitoring therapeutic efficacy.

A common strategy for multimodal apoptosis imaging is by designing a probe that is activated after caspase-mediated self-assembly into NPs. Wang et al. used this strategy to create a PA and FL imaging caspase-3 responsive probe (1-RGD).[72] A peptide sequence in the 1-RGD probe was cleaved by caspase-3 and induced macrocyclization that resulted in NP self-assembly. Incubating 1-RGD with caspase-3 eliminated FL signal and enhanced PA signal intensity. Additionally, the specificity of this design was demonstrated by incubating caspase-3 with a caspase-3 inhibitor (Z-VAD-fmk) and 1-RGD, which resulted in no PA signal enhancement or FL signal elimination. In vivo imaging studies after intravenous injection of 1-RGD found that mice with U87MG subcutaneous tumors and treated with doxorubicin had enhanced PA signal compared to controls. Thus, this strategy was able to visualize chemotherapy-induced apoptosis throughout the tumor to monitor treatment efficacy.

It is always more advantageous to employ activatable imaging strategies with contrast that is enhanced in response to a stimulus. Meade and co-workers prepared a caspase-3/7 activatable FL/MR contrast agent where both signals were enhanced after activation.[73] This fluorogenic caspase probe (CP1) combined a Gd^{3+}-chelate, a tetraphenylethylene unit for aggregation-induced emission luminogen (AIEgen), and a caspase-3/7 cleavable substrate (DEVD peptide). Once the DVED peptide is cleaved by caspase-3/7, the remaining Gd^{3+}-chelate-AIEgen moieties aggregated together. The aggregation and NP formation increased both the FL and MR signal intensity compared to minimal changes with a non-caspase-cleavable control probe. Interestingly, the authors were able to correlate the FL emission and CP1 concentration to predict the T_1-weighted MR signal in vitro accurately. In vivo application of this probe could visualize caspase expression in response to treatments and be further adapted for imaging activation of other targets.

3.3.4. Other Enzymes—Any number of enzymes could theoretically be used as a stimulus for activatable imaging, as long it was overexpressed in neoplastic tissue. Alkaline phosphatase (ALP) is an enzyme that exists in both healthy and cancerous tissue that acts by dephosphorylating compounds.[74] Overexpression of ALP has been found on various cancer cell lines, which enables strategies that are selectively activated by this enzyme.[75] Typically, small molecules are used that form NPs after dephosphorylated by ALP.[76] As an example, the Liang group synthesized a NIR probe with an enhanced PA signal and quenched FL signal after activated by ALP.[77] This nanosystem permitted a highly sensitive diagnosis of superficial tumors. In another design, Zhang and co-workers reported a prostate cancer imaging platform using an ALP-activatable and mitochondria-targeted probe.[78] The FL and PA intensity of the probe (ETP), composed of a NIR FL dye, a lipophilic triphenylphosphium cation that targets mitochondria, and a phosphate ester group, was drastically increased after incubating with ALP. The enhancement was attributed to the removal of the phosphate group that quenched FL/PA signal and resulted in situ NPs self-

assembly. In vivo NIRF and PA imaging studies found that the ETP probe could visualize PC-3 tumors, with specificity demonstrated by decreased signal after treatment with an ALP inhibitor.

Recently. Yan et al. prepared a small-molecule-based activatable NIRF/MR (fluorogenic MR) bimodal imaging probe that would self-assemble into NPs in situ once activated by ALP (Figure 9a).[64] Since the probe was prepared as a small molecule, it may pass through blood vasculature and penetrate tumors better than similarly designed NPs. Another advantage of administering a small molecule is that any unactivated P-CyFF-Gd would likely be eliminated in vivo. Their probe was constructed by combining a prequenched fluorophore (merocyanine) capped with an ALP cleavable phosphate group with a Gd-DOTA chelate for MR imaging and a hydrophobic dipeptide Phe-Phe linker for self-assembly (P-CyFF-Gd). When this hydrophilic probe is administered in vivo and encounters ALP, the phosphate cap on the fluorophore was cleaved by dephosphorylation producing hydrophobic CyFF-Gd that self-assembled through π–π interactions. Incubating P-CyFF-Gd with ALP induced a more than 70-fold increase in FL intensity and an r_1 increase from 8.9 ± 0.3 to 20.1 ± 0.5 mM^{-1} s^{-1} due to the increased NP size with a longer tumbling time and restricted molecular motion. Enzyme kinetic studies found that P-CyFF-Gd was a suitable substrate for ALP with a V_{max} of 1.05×10^{-6} M min^{-1}, K_m of 13.14×10^{-6} M, and a k_{cat}/K_m ratio of 3.6×10^4 M^{-1} s^{-1}. Initial in vivo imaging investigated subcutaneous injection of P-CyFF-Gd with or without ALP. FL intensity and MR signal of P-CyFF-Gd and ALP peaked 1 h p.i. and was significantly higher than P-CyFF-Gd alone, due to the combination of decreased activation and elimination of the small molecule. Subcutaneous HeLa tumor-bearing mice were then used to visualize endogenous ALP with P-CyFF-Gd. Following intravenous injection of P-CyFF-Gd (50×10^{-6} M), FL intensity and T_1-weighted contrast peaked at 1 h and 4 h p.i., respectively (Figure 9b,c). Inhibiting ALP activity (Na_3VO_4) or removing the ALP substrate (P-Cy-Gd) dramatically reduced signal from both modalities. With the encouraging imaging results, P-CyFF-Gd was employed for surgical resection of luciferase transfected orthotopic liver tumors (HepG2/Luc). Imaging using the orthotopic model after intravenous injection of P-CyFF-Gd, shown in Figure 9d,e, yielded T_1-weighted MR images that delineated the tumor from surrounding tissue and NIRF images that correlated with bioluminescence signal from the cancer cells. Orthotopic tumors were then removed surgically after spraying P-CyFF-Gd on the tumor containing liver, which was visualized by NIRF imaging after 30 min (Figure 9f). The in situ NP assembly strategy used in this study provided the context of ALP activity in tumors while simultaneously yielding structural information of ALP-positive tumor tissues that could be extended for surgical resection of tumors.

Hyaluronic acid (HA)-based materials have been widely used in drug delivery and imaging applications.[79] Extensive research has shown that HA can actively target CD44, which is expressed on many different tumor types.[80] Importantly, HA can be degraded by hyaluronidase-1 (Hyal-1), which is the basis for activatable multimodal imaging applications. In a conventional method, degradation of the HA-based material will liberate the nanoprobe from a quenched state and functionalized with other compounds for multimodal functionality.[80]

A Hyal-1-activated probe was prepared by Wang and co-workers.[81] In their design, Cy5.5 and IR825 were conjugated HA to form a nanoprobe that was then encapsulated with perfluorooctylbromide (PFOB), which absorbs X-rays (PFOB@IR825-HA-Cy5.5). Due to the proximity of Cy5.5 to IR825, FL signal was initially quenched. Once the PFOB@IR825-HA-Cy5.5 substrate interacted with Hyal-1, the HA backbone was degraded, and the FL intensity dramatically increased. The other components of the nanosystem, IR825 and PFOB, enabled PA and CT imaging. PFOB@IR825-HA-Cy5.5 was intravenously injected into HT-29 (CD 44 positive) tumor xenograft model. Enhanced FL signal from CD44 activation reached a maximum in the tumor at 24 h p.i. and was relatively low in the other major organs of interest. Similarly, the PA amplitude in the tumor tissue clearly visualized the tumor as early as 1 h p.i and approached the maximum (at 24 h) as soon as 5 h p.i. CT imaging studies also found that the tumor could be clearly delineated. FL activation of PFOB@IR825-HA-Cy5.5 by Hyal-1 resulted in continuous signal enhancement up to 24 h p.i., whereas PA and CT contrast rapidly peaked and remained steady in the 5 h to 48 h p.i. timeframe. This trimodal system was able to actively target CD44 positive tumors and delineate them once activated by Hyal-1.

3.4. Multi-Responsive

Designing nanomaterials that respond to multiple stimuli can further expand imaging capabilities. Commonly, nanomaterials are found to be simultaneously responsive to pH and redox potential. This typically occurs as a result of the inherent properties of a material or by including various moieties sensitive to stimuli. In this section, we discuss nanoprobes that are activated by simultaneous stimuli.

The pH gradient and reductive environment that exist in tumors are frequently exploited to synergistically enhance image contrast. In an acidic and H_2O_2-rich environment, MnO_2-based nanomaterials will react according to the following equation: $H_2O_2 + 2H^+ MnO_2 \rightarrow 2H_2O + O_2 + Mn^{2+}$, which enhances T_1-weighted MR contrast due to the increase in Mn^{2+} concentration.[82] Preparing MnO_2 NPs as the core or coating nanomaterials with a MnO_2 layer or MnO_2 NPs are both effective methods to capitalize on this strategy. The Yang group prepared honeycomb manganese oxide nanospheres as a core that were functionalized with Ce6-conjugated core-shell UCNPs (hMUC).[83] In the presence of hydrogen peroxide and slightly acidic conditions, the hMUCs were degraded, and the UCNPs-Ce6 was released from the surface. The benefits of this were twofold, the release of UCNPs-Ce6 enhanced its ability to absorb light and increased Mn^{2+} concentration for activatable MR imaging, which was combined with CT imaging to visualize the tumor structure. In another study, Hu et al. developed an intelligent polymer platform that was conjugated with MnO_2 NPs and BIODIPY molecules.[84] Once surface-functionalized MnO_2 NPs were degraded, the MR signal and PA ratio (825/680 nm) signal was enhanced and enabled the delineation of 4T1 tumors. It is also worth mentioning that O_2 is produced in this strategy, which may decrease tumor hypoxia and increase the efficacy of therapeutic strategies.

As we have mentioned, MnO_2-based nanoprobes can also be degraded by GSH, which can be combined to respond with changes in pH and H_2O_2 concentrations. Jing et al. showed that an intelligent nanoflower composite (FHCPC@MnO_2) could exploit the low pH and

high levels of H_2O_2 and GSH that exist in the TME (Figure 10a).[85,86] IONP nanoclusters were encapsulated with a GSH and a pH-responsive polyphosphazene (PPZ)-drug conjugate layer and was then coated with a MnO_2 shell. In a slightly acidic, H_2O_2 and GSH-rich environment, the MnO_2 and PPZ layers were degraded. As a result of the FHCPC@MnO_2 composition, the T_1- and T_2-weighted MR imaging was enhanced for anatomical contrast that could be simultaneously paired with FL imaging (Figure 10b,c). In another study, the Tan group achieved activatable FL and MR imaging using mesoporous silica and gelatin nanolayer protected MnO_2 coated UCNPs.[87] When the pH was decreased and GSH levels increased, a remarkable increase in the T_1-weighted contrast and UCL was observed. Importantly, the protection layers included in this design were effective at preventing premature reduction of MnO_2 in blood, which is a significant limitation of MnO_2-based nanomaterials.

Recently, a hybrid protein@inorganic nanodumpling (ND) system was prepared by Zhu et al. for biothiol and pH activatable FL and MR imaging using a green and straightforward process (Figure 10d).[88] In their design, functional proteins were fused with a 39-histidine base-green fluorescent protein (H_{39}GFP) tag to enable zinc ion directed self-assembly as the "filling." The fabricated protein complex was then coated using in situ biomineralization with a MnO_2 "wrapper" and then PEGylated with a FA-containing moiety for enhanced circulation and biocompatibility as well as endow folate receptor targeting (H_{39}GFP@MnO_2 NDs). The MnO_2 coating served to protect the internal protein cargo from premature release. Additionally, the decreased pH and elevated GSH in the TME triggered the disassociation of the MnO_2 layer, providing responsiveness. Since MnO_2 quenches FL emission from GFP before degradation, the H_{39}GFP@MnO_2 NDs enable FL imaging and MR imaging from increased Mn^{2+} once activated. To model this carrier, the H_{39}GFP was fused with a NIRF protein (IRFP, Ex/Em = 683/703 nm; IRFP-H_{39}GFP@MnO_2 NDs). In vivo FL and MR imaging were then used to monitor protein delivery in HCT 116 xenograft tumor-bearing mice (FR-positive). Intravenous injection of IRFP-H_{39}GFP@MnO_2 NDs resulted in a FL signal maximum 4 h p.i. and correlated with a peak tumor-to-normal tissue (T/N) contrast enhancement of 167% at the same timepoint in T_1-weighted MR images. In comparison, nonspecific FL signal and negligible T/N contrast increase when free protein was administered. Extension of these imaging modalities provided visualization of ribonuclease A-fused NDs, a protein that is cytotoxic.

Other multi-responsive multimodal imaging agents can be prepared by careful incorporation of various pH-, H_2O_2-, or GSH-responsive components into a single nanoplatform. Wu et al. demonstrated this strategy using a multifunctional, biodegradable, hollow mesoporous organosilica nanocapule (HMONS). pH- and GSH-mediated release and degradation of HMONS were observed due to conjugation with pH-cleavable acetal covalent bonds and incorporated disulfide bonds. Tumors could be delineated with this nanoprobe using PA and FL imaging. While this and the previously mentioned examples of multi-responsive agents have many advantages, it also complicates multimodal imaging applications.

4. Conclusion

A significant advancement in nanomedicine has been the development of activatable multimodal imaging agents. This can be achieved by taking advantage of the slightly acidic pH, high GSH and ROS levels, overexpression of enzymes, or combinations of these conditions that all exist in the TME. Compared to “always-on” imaging agents, specific activation to one or more of these stimuli improves the tumor-to-background ratio across one or more imaging modalities. Additionally, using multiple imaging modalities combines complementary anatomical and biological information, making these features easier to distinguish or highlight. Ultimately, the diagnostic performance of nanomaterials can be improved while simultaneously reducing side effects. Applying nanomaterials for activatable multimodal imaging can provide noninvasive cancer diagnosis in real-time as well as a method to monitor treatment regimens and drug distribution.

Acknowledgements

This work was supported, in part, by the University of Wisconsin-Madison and the National Institutes of Health (P30CA014520).

Biography

Zachary T. Rosenkrans is currently a Ph.D. student in the Pharmaceutical Sciences program at the University of Wisconsin-Madison, under the supervision of Prof. Weibo Cai. He previously received a B.S. in chemical engineering from the University of Kansas in Lawrence, KS. His research focuses on developing nanomaterial-based platforms for image-guided drug delivery and theranostics.

Dalong Ni received his Ph.D. degree in 2016 from the Shanghai Institute of Ceramics, Chinese Academy of Sciences (SICCAS). Hethen joined the Department of Radiology at the University of Wisconsin-Madison as a postdoctoral fellow under the supervision of Prof. Weibo Cai. His research interests focus on design, synthesis, and biomedical applications of multifunctional nanoplatforms for imaging and therapy applications.

Weibo Cai is a Vilas Distinguished Achievement Professor of Radiology/Medical Physics/Biomedical Engineering/Materials Science and Engineering/Pharmaceutical Sciences at the University of Wisconsin-Madison, USA. He received a Ph.D. degree in Chemistry from UCSD in 2004. Prof. Cai's research at UW-Madison (http://mi.wisc.edu/) is mainly focused on antibody-based molecular imaging and nanotechnology. He has authored >300 articles (H-index: 79), edited three books, and received many awards (e.g., Fellow of AIMBE in 2018 and Fellow of SNMMI in 2019). Prof. Cai's trainees at UW-Madison have received >100 awards.

References

[1]. a)James ML, Gambhir SS, Physiol. Rev 2012, 92, 897; [PubMed: 22535898] b)Fass L, Mol. Oncol 2008, 2, 115. [PubMed: 19383333]

[2]. Histed SN, Lindenberg ML, Mena E, Turkbey B, Choyke PL, Kurdziel KA, Nucl. Med. Commun 2012, 33, 349. [PubMed: 22314804]

[3]. a)Weissleder R, Mahmood U, Radiology 2001, 219, 316; [PubMed: 11323453] b)Frangioni JV, Clin J. Oncol. 2008, 26, 4012.

[4]. Weissleder R, Pittet MJ, Nature 2008, 452, 580. [PubMed: 18385732]

[5]. Cai W, Chen X, J. Nucl. Med 2008, 49, 113S. [PubMed: 18523069]

[6]. a)Hu Q, Chen Q, Gu Z, Biomaterials 2018, 178, 546; [PubMed: 29657093] b)Zhang J, Yuan Z-F, Wang Y, Chen W-H, Luo G-F, Cheng S-X, Zhuo R-X, Zhang X-Z, J. Am. Chem. Soc 2013, 135, 5068; [PubMed: 23464924] c)He Q, Shi J, J. Mater. Chem 2011, 21, 5845.

[7]. a)Lee D-E, Koo H, Sun I-C, Ryu JH, Kim K, Kwon IC, Chem. Soc. Rev 2012, 41, 2656; [PubMed: 22189429] b)Ni D, Ehlerding EB, Cai W, Angew. Chem., Int. Ed 2019, 58, 2570.

[8]. Kang T, Li F, Baik S, Shao W, Ling D, Hyeon T, Biomaterials 2017, 136, 98. [PubMed: 28525855]

[9]. Lu Y, Aimetti AA, Langer R, Gu Z, Nat. Rev. Mater 2017, 2, 16075.

[10]. a)Qiao Y, Wan J, Zhou L, Ma W, Yang Y, Luo W, Yu Z, Wang H, Wiley Interdiscip. Rev.: Nanomed. Nanobiotechnol 2019, 11, e1527; [PubMed: 29726115] b)Li X, Kim J, Yoon J, Chen X, Adv. Funct. Mater 2014, 24, 4206; [PubMed: 25477774] c)Wang Y, Shim MS, Levinson NS, Sung H-W, Xia Y, Adv. Funct. Mater 2014, 24, 4206. [PubMed: 25477774]

[11]. Wang Y, Song S, Lu T, Cheng Y, Song Y, Wang S, Tan F, Li J, Li N, Biomaterials 2019, 220, 119405. [PubMed: 31408811]

[12]. a)S. M. M, Veeranarayanan S, Maekawa T, S. K. D, Adv. Drug Delivery Rev 2019, 138, 18;b)Zhou L, Wang H, Li Y, Theranostics 2018, 8, 1059. [PubMed: 29463999]

[13]. Wu T, Dai Y, Cancer Lett. 2017, 387, 61. [PubMed: 26845449]

[14]. a)Tong R, Langer R, Cancer J. 2015, 21, 314; [PubMed: 26222084] b)Hui L, Chen Y, Cancer Lett. 2015, 368, 7. [PubMed: 26276713]

[15]. Cairns RA, Harris IS, Mak TW, Nat. Rev. Cancer 2011, 11, 85. [PubMed: 21258394]

[16]. Yu J, Chu X, Hou Y, Chem. Commun 2014, 50, 11614.

[17]. Sosa V, Moliné T, Somoza R, Paciucci R, Kondoh H, Lleonart ME, Ageing Res. Rev 2013, 12, 376. [PubMed: 23123177]

[18]. Meng F, Hennink WE, Zhong Z, Biomaterials 2009, 30, 2180. [PubMed: 19200596]

[19]. de la Rica R, Aili D, Stevens MM, Adv. Drug Delivery Rev 2012, 64, 967.

[20]. Kanamala M, Wilson WR, Yang M, Palmer BD, Wu Z, Biomaterials 2016, 85, 152. [PubMed: 26871891]

[21]. Wei R, Gong X, Lin H, Zhang K, Li A, Liu K, Shan H, Chen X, Gao J, Nano Lett. 2019, 19, 5394. [PubMed: 31286778]

[22]. Hsu BYW, Ng M, Tan A, Connell J, Roberts T, Lythgoe M, Zhang Y, Wong SY, Bhakoo K, Seifalian AM, Li X, Wang J, Adv. Healthcare Mater 2016, 5, 721.

[23]. Liu Y, Lv X, Liu H, Zhou Z, Huang J, Lei S, Cai S, Chen Z, Guo Y, Chen Z, Zhou X, Nie L, Nanoscale 2018, 10, 3631. [PubMed: 29412212]

[24]. Dong Z, Feng L, Zhu W, Sun X, Gao M, Zhao H, Chao Y, Liu Z, Biomaterials 2016, 110, 60. [PubMed: 27710833]

[25]. Dong Z, Feng L, Hao Y, Chen M, Gao M, Chao Y, Zhao H, Zhu W, Liu J, Liang C, Zhang Q, Liu Z, J. Am. Chem. Soc 2018, 140, 2165. [PubMed: 29376345]

[26]. Wang S, Zhou Z, Yu G, Lu N, Liu Y, Dai Y, Fu X, Wang J, Chen X, ACS Appl. Mater. Interfaces 2018, 10, 28382. [PubMed: 30085649]

[27]. Li J, Liu C, Hu Y, Ji C, Li S, Yin M, Theranostics 2020, 10, 166. [PubMed: 31903113]

[28]. Wang T, Wang D, Yu H, Wang M, Liu J, Feng B, Zhou F, Yin Q, Zhang Z, Huang Y, Li Y, ACS Nano 2016, 10, 3496. [PubMed: 26866752]

[29]. Ling D, Park W, Park S-J, Lu Y, Kim KS, Hackett MJ, Kim BH, Yim H, Jeon YS, Na K, Hyeon T, J. Am. Chem. Soc 2014, 136, 5647. [PubMed: 24689550]

[30]. Li Y, Lin J, Wang P, Luo Q, Lin H, Zhang Y, Hou Z, Liu J, Liu X, ACS Nano 2019, 13, 12912. [PubMed: 31651142]

[31]. Gao M, Fan F, Li D, Yu Y, Mao K, Sun T, Qian H, Tao W, Yang X, Biomaterials 2017, 133, 165. [PubMed: 28437627]

[32]. Tang Y, Shi H, Cheng D, Zhang J, Lin Y, Xu Y, Qian X, Zhu W, Colloids Surf., B 2019, 179, 56.

[33]. Yu K-K, Li K, Lu C-Y, Xie Y-M, Liu Y-H, Zhou Q, Bao J-K, Yu X-Q, Nanoscale 2020, 12, 2002.

[34]. Zhang P, Hou Y, Zeng J, Li Y, Wang Z, Zhu R, Ma T, Gao M, Angew. Chem., Int. Ed 2019, 58, 11088.

[35]. Traverso N, Ricciarelli R, Nitti M, Marengo B, Furfaro AL, Pronzato MA, Marinari UM, Domenicotti C, Oxid. Med. Cell. Longevity 2013, 2013, 1.

[36]. Balendiran GK, Dabur R, Fraser D, Cell Biochem. Funct. 2004, 22, 343. [PubMed: 15386533]

[37]. Mura S, Nicolas J, Couvreur P, Nat. Mater. 2013, 12, 991. [PubMed: 24150417]

[38]. Guo X, Cheng Y, Zhao X, Luo Y, Chen J, Yuan W-E, J. Nanobiotechnol 2018, 16, 74.

[39]. Mitra RN, Doshi M, Zhang X, Tyus JC, Bengtsson N, Fletcher S, Page BDG, Turkson J, Gesquiere AJ, Gunning PT, Walter GA, Santra S, Biomaterials 2012, 33, 1500. [PubMed: 22078810]

[40]. Hu D, Sheng Z, Gao G, Siu F, Liu C, Wan Q, Gong P, Zheng H, Ma Y, Cai L, Biomaterials 2016, 93, 10. [PubMed: 27061266]

[41]. Zheng M, Wang Y, Shi H, Hu Y, Feng L, Luo Z, Zhou M, He J, Zhou Z, Zhang Y, Ye D, ACS Nano 2016, 10, 10075. [PubMed: 27934082]

[42]. Clore GM, Iwahara J, Chem. Rev 2009, 109, 4108. [PubMed: 19522502]

[43]. Chen Y, Ye D, Wu M, Chen H, Zhang L, Shi J, Wang L, Adv. Mater 2014, 26, 7019. [PubMed: 25156250]

[44]. Yuan D, Ding L, Sun Z, Li X, Sci. Rep 2018, 8, 1747. [PubMed: 29379132]

[45]. Zhao Z, Fan H, Zhou G, Bai H, Liang H, Wang R, Zhang X, Tan W, J. Am. Chem. Soc 2014, 136, 11220. [PubMed: 25061849]

[46]. a)Fan H, Zhao Z, Yan G, Zhang X, Yang C, Meng H, Chen Z, Liu H, Tan W, Angew. Chem., Int. Ed 2015, 54, 4801;b)Fan H, Yan G, Zhao Z, Hu X, Zhang W, Liu H, Fu X, Fu T, Zhang XB, Tan W, Angew. Chem., Int. Ed 2016, 55, 5477.

[47]. a)Gamcsik MP, Kasibhatla MS, Teeter SD, Colvin OM, Biomarkers 2012, 17, 671; [PubMed: 22900535] b)Burhans WC, Heintz NH, Free Radical Biol. Med 2009, 47, 1282. [PubMed: 19486941]

[48]. Ferreira CA, Ni D, Rosenkrans ZT, Cai W, Nano Res. 2018, 11, 4955. [PubMed: 30450165]

[49]. Liou G-Y, Storz P, Free Radical Res. 2010, 44, 479. [PubMed: 20370557]

[50]. Zhang L, Chen Q, Zou X, Chen J, Hu L, Dong Z, Zhou J, Chen Y, Liu Z, Cheng L, J. Mater. Chem. B 2019, 7, 5170. [PubMed: 31384859]

[51]. Peng J, Dong M, Ran B, Li W, Hao Y, Yang Q, Tan L, Shi K, Qian Z, ACS Appl. Mater. Interfaces 2017, 9, 13875. [PubMed: 28374581]

[52]. Bouché M, Pühringer M, Iturmendi A, Amirshaghaghi A, Tsourkas A, Teasdale I, Cormode DP, ACS Appl. Mater. Interfaces 2019, 11,28648. [PubMed: 31321973]

[53]. Cheong H, Lu C, Lindsten T, Thompson CB, Nat. Biotechnol 2012, 30, 671. [PubMed: 22781696]

[54]. Isaacson KJ, Jensen MM, Subrahmanyam NB, Ghandehari H, J. Controlled Release 2017, 259, 62.

[55]. Gao S, Zhang L, Wang G, Yang K, Chen M, Tian R, Ma Q, Zhu L, Biomaterials 2016, 79, 36. [PubMed: 26691399]

[56]. Turpeenniemi-Hujanen T, Biochimie 2005, 87, 287. [PubMed: 15781315]

[57]. Olson ES, Jiang T, Aguilera TA, Nguyen QT, Ellies LG, Scadeng M, Tsien RY, Proc. Natl. Acad. Sci. USA 2010, 107, 4311. [PubMed: 20160077]

[58]. Cha E-J, Jang ES, Sun I-C, Lee IJ, Ko JH, Kim YI, Kwon IC, Kim K, Ahn C-H, J. Controlled Release 2011, 155, 152.

[59]. Shi H, Sun Y, Yan R, Liu S, Zhu L, Liu S, Feng Y, Wang P, He J, Zhou Z, Ye D, Nano Lett. 2019, 19, 937. [PubMed: 30688465]

[60]. Chen S, Cui J, Jiang T, Olson ES, Cai Q-Y, Yang M, Wu W, Guthrie JM, Robertson JD, Lipton SA, Ma L, Tsien RY, Gu Z, Cereb J. Blood Flow Metab. 2017, 37, 188.

[61]. Di Cera E, IUBMB Life 2009, 61, 510. [PubMed: 19180666]

[62]. Li X, Bottini M, Zhang L, Zhang S, Chen J, Zhang T, Liu L, Rosato N, Ma X, Shi X, Wu Y, Guo W, Liang X-J, ACS Nano 2019, 13, 176. [PubMed: 30592401]

[63]. Park JE, Lenter MC, Zimmermann RN, Garin-Chesa P, Old LJ, Rettig WJ, J. Biol. Chem 1999, 274, 36505. [PubMed: 10593948]

[64]. Han X, Xu Y, Li Y, Zhao X, Zhang Y, Min H, Qi Y, Anderson GJ, You L, Zhao Y, Nie G, ACS Nano 2019, 13, 4379. [PubMed: 30901191]

[65]. Brennen WN, Isaacs JT, Denmeade SR, Mol. Cancer Ther 2012, 11, 257. [PubMed: 22323494]

[66]. Rickles FR, Patierno S, Fernandez PM, Chest 2003, 124, 58S. [PubMed: 12970125]

[67]. Kwon S-P, Jeon S, Lee S-H, Yoon HY, Ryu JH, Choi D, Kim J-Y, Kim J, Park JH, Kim D-E, Kwon IC, Kim K, Ahn C-H, Biomaterials 2018, 150, 125. [PubMed: 29035738]

[68]. Ouyang L, Shi Z, Zhao S, Wang F-T, Zhou T-T, Liu B, Bao J-K, Cell Proliferation 2012, 45, 487. [PubMed: 23030059]

[69]. Fiandalo MV, Kyprianou N, Exp. Oncol 2012, 34, 165. [PubMed: 23070001]

[70]. Thornberry NA, Lazebnik Y, Science 1998, 281, 1312. [PubMed: 9721091]

[71]. Li J, Yuan J, Oncogene 2008, 27, 6194. [PubMed: 18931687]

[72]. Wang Y, Hu X, Weng J, Li J, Fan Q, Zhang Y, Ye D, Angew. Chem., Int. Ed 2019, 58, 4886.

[73]. Li H, Parigi G, Luchinat C, Meade TJ, J. Am. Chem. Soc 2019, 141, 6224. [PubMed: 30919628]

[74]. McComb RB, Bowers GN Jr., Posen S, Alkaline Phosphatase, Springer Science & Business Media, Berlin 2013.

[75]. a)Nowrouzi A, Yazdanparast R, Biochem. Biophys. Res. Commun 2005, 330, 400; [PubMed: 15796897] b)Fishman WH, Inglis NR, Green S, Anstiss CL, Gosh NK, Reif AE, Rustigian R, Krant MJ, Stolbach LL, Nature 1968, 219, 697. [PubMed: 5691166]

[76]. Zhan J, Cai Y, He S, Wang L, Yang Z, Angew. Chem., Int. Ed 2018, 57, 1813.

[77]. Wu C, Zhang R, Du W, Cheng L, Liang G, Nano Lett. 2018, 18, 7749. [PubMed: 30481463]

[78]. Yao D, Yang S, Wang Y, Bian K, Yang W, Wang D, Zhang B, Nanoscale 2019, 11, 6307. [PubMed: 30882834]

[79]. Choi KY, Han HS, Lee ES, Shin JM, Almquist BD, Lee DS, Park JH, Adv. Mater 2019, 31, 1803549.

[80]. Zhang L, Gao S, Zhang F, Yang K, Ma Q, Zhu L, ACS Nano 2014, 8, 12250. [PubMed: 25402600]

[81]. Liang X, Fang L, Li X, Zhang X, Wang F, Biomaterials 2017, 132, 72. [PubMed: 28411450]

[82]. Liang R, Liu L, He H, Chen Z, Han Z, Luo Z, Wu Z, Zheng M, Ma Y, Cai L, Biomaterials 2018, 177, 149. [PubMed: 29890364]

[83]. Sun Q, He F, Sun C, Wang X, Li C, Xu J, Yang D, Bi H, Gai S, Yang P, ACS Appl. Mater. Interfaces 2018, 10, 33901. [PubMed: 30207691]

[84]. Hu X, Zhan C, Tang Y, Lu F, Li Y, Pei F, Lu X, Ji Y, Li J, Wang W, Fan Q, Huang W, Chem. Commun 2019, 55, 6006.

[85]. Jing X, Zhi Z, Wang D, Liu J, Shao Y, Meng L, Bioconjugate Chem. 2018, 29, 559.

[86]. Jing X, Xu Y, Liu D, Wu Y, Zhou N, Wang D, Yan K, Meng L, Nanoscale 2019, 11, 15508. [PubMed: 31393496]

[87]. Wu Y, Li D, Zhou F, Liang H, Liu Y, Hou W, Yuan Q, Zhang X, Tan W, Chem. Sci 2018, 9, 5427. [PubMed: 30009014]

[88]. Zhu X, Tang R, Wang S, Chen X, Hu J, Lei C, Huang Y, Wang H, Nie Z, Yao S, ACS Nano 2020, 14, 2172. [PubMed: 31990525]

[89]. Yan R, Hu Y, Liu F, Wei S, Fang D, Shuhendler AJ, Liu H, Chen H-Y, Ye D, J. Am. Chem. Soc 2019, 141, 10331. [PubMed: 31244188]

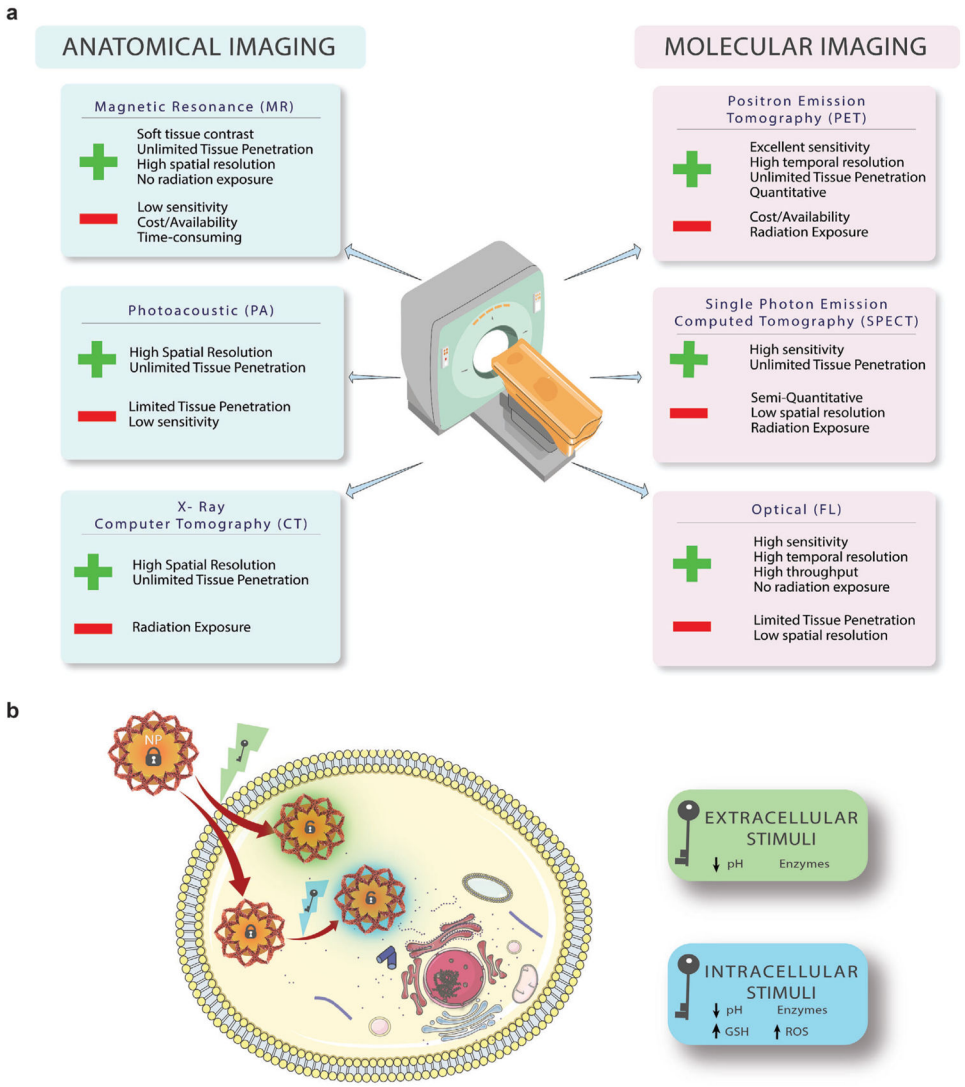

Figure 1.

Internally responsive activatable multimodal imaging. a) Multimodal imaging combines advantages and disadvantages of various anatomical and molecular imaging modalities. FL refers to fluorescence imaging. b) Internally responsive multimodal imaging nanomaterials are activated by pH gradients, redox potential, enzymes, or combinations of these. NP, GSH, and ROS refer to nanoparticle, glutathione, and reactive oxygen species, respectively.

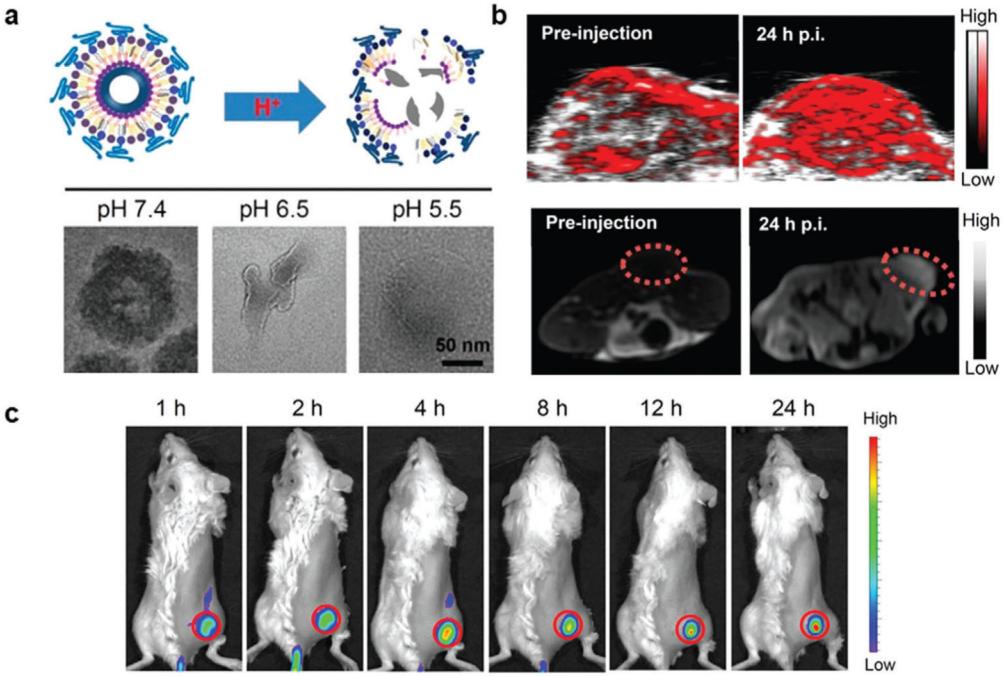

Figure 2.

pH-activatable multimodal imaging by nanomaterial degradation. a) Calcium carbonate ($CaCO_3$) NPs were synthesized with a polydopamine coating that degraded under slightly acidic conditions (upper). TEM images confirmed this under different pH conditions (lower). b) $CaCO_3$ NPs absorbed NIR light for PA imaging (upper) and chelated metal ions for MR imaging (lower). c) Degradation of the $CaCO_3$ backbone reduced polydopamine FL quenching of Ce6 for activated FL imaging. Reproduced with permission.[25] Copyright 2018, American Chemical Society.

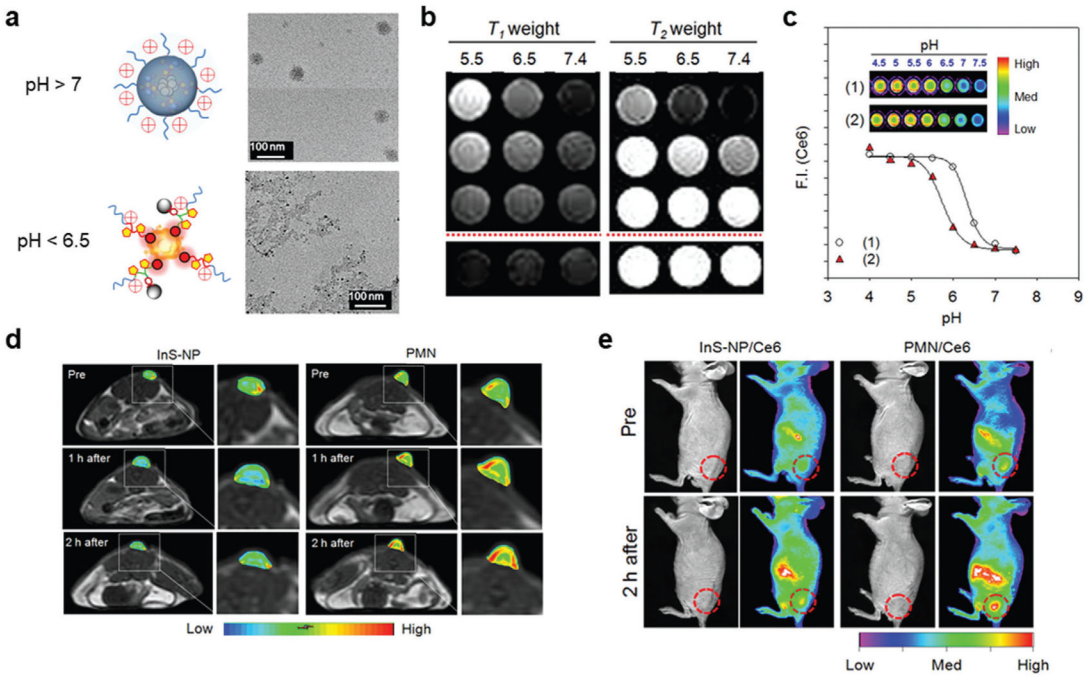

Figure 3.

pH-activatable multimodal imaging by amine protonation. a) PMNs were composed of ESIONs that were self-assembled with a Ce6 and imidazole containing ligands. In a reversible process, the imidazole in the PMNs was protonated as the pH of the environment decreased, causing the nanosystem to swell and ultimately disassemble, as shown in TEM images. b,c) As a result, both the MR contrast and FL intensity of PMNs were dependent upon pH. e,f) InS-NP and InS-NP/Ce6 are nonresponsive probes that demonstrate the advantages of the pH-activated PMNs. Reproduced with permission.[29] Copyright 2014, American Chemical Society.

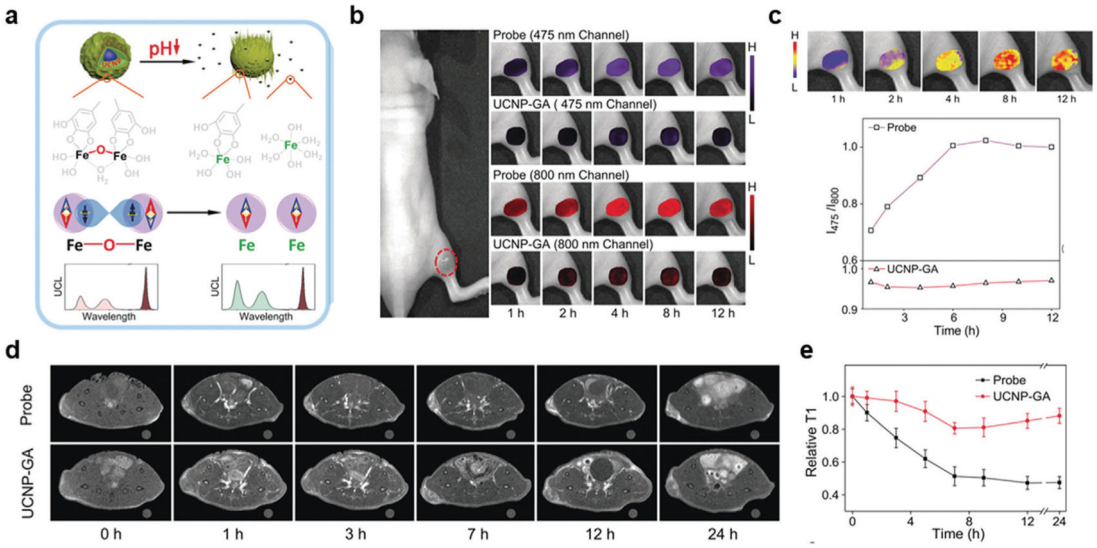

Figure 4.

pH-activatable multimodal imaging incorporating an acid liable group. a) In slightly acidic conditions, FL and MR activation of the nanoprobes occurred after releasing a Fe^{III}-containing moiety. b,c) The release of the Fe^{III}-containing moiety could be monitored in vivo by the ratio of the emissions at 475 and 800 nm (I_{475}/I_{800}). d) T_1-weighted MR images and e) corresponding analysis. In (b)–(e), probe was the pH-activatable nanoprobe and UCNP-GA was a nonresponsive control for comparison. Reproduced with permission.[34] Copyright 2019, Wiley.

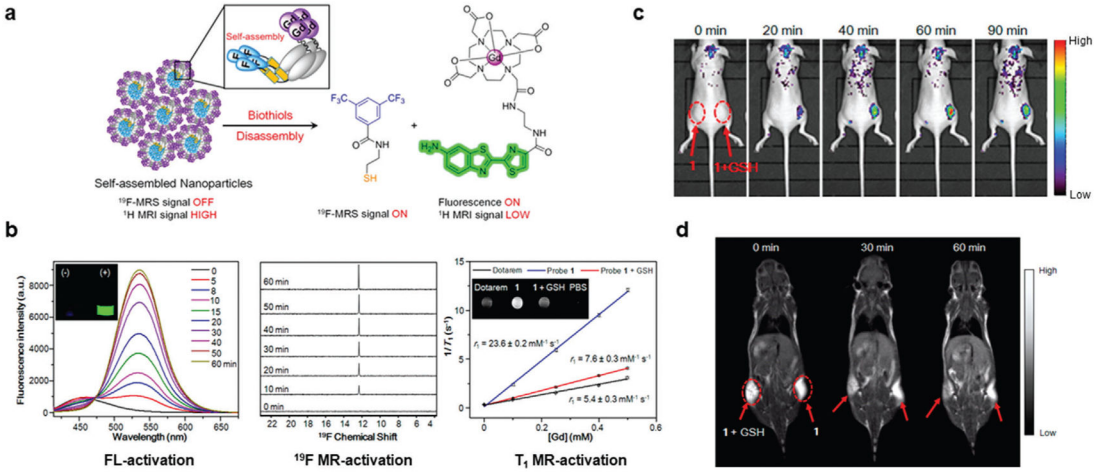

Figure 5.

GSH-activated multimodal imaging. a) NPs were self-assembled from a compound containing a ^{19}F-MRS signal moiety, a Gd-DOTA chelate, and a disulfide-capped fluorophore. b) When incubated with GSH, the disulfide bond in the self-assembled NPs was cleaved. As a result, the disassembled NPs displayed activated FL (left), ^{19}F-MR (middle), and T_1-weighted MR (right) signals. Reproduced with permission.[41] Copyright 2016, American Chemical Society.

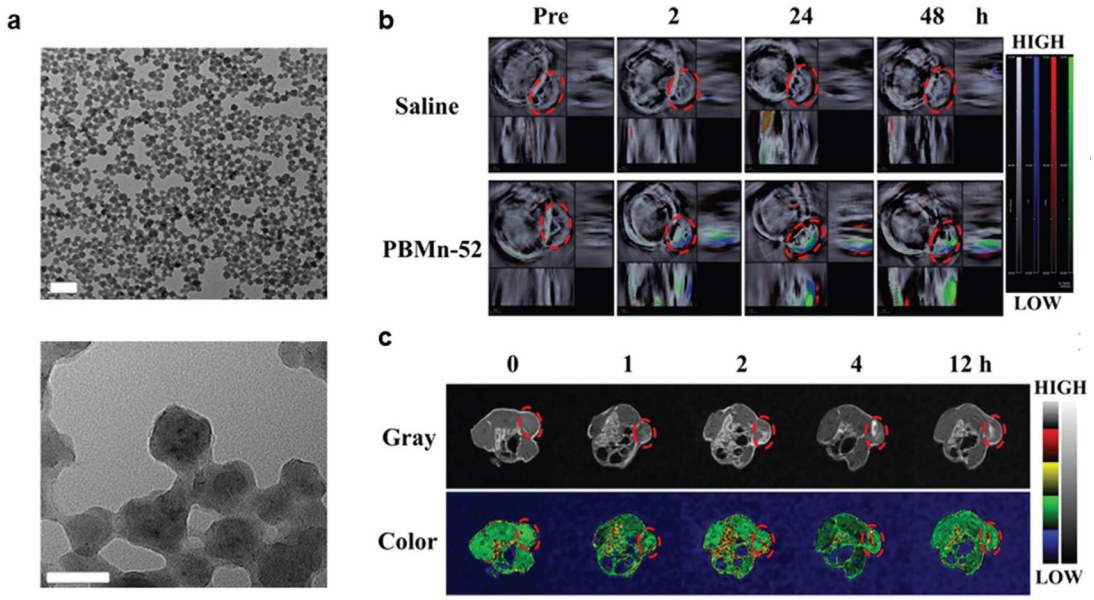

Figure 6.

H_2O_2-activated multimodal imaging. a) TEM images of PBMn-52 hybrid nanocrystals. Scale bar: 200 nm (top) and 50 nm (bottom). b) In vivo PA imaging and c) activatable T_1-weighted MR imaging demonstrated that PBMn-52 was an effective contrast agent. Reproduced with permission.[51] Copyright 2017, American Chemical Society.

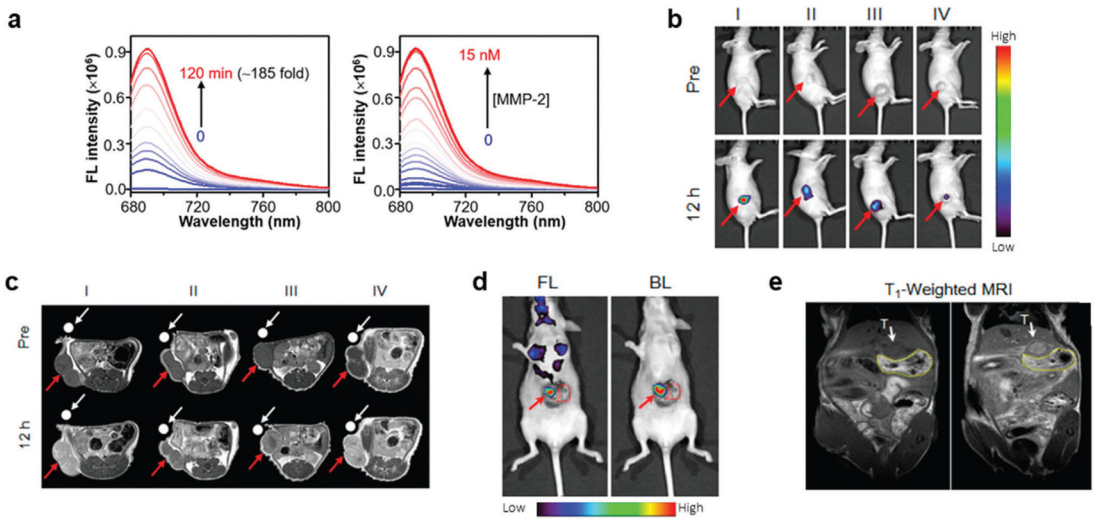

Figure 7.

Matrix metallopeptidase-2 (MMP-2)-activated multimodal imaging. a) MMP-2 mediated cleavage of T-MAN enhanced the FL intensity. In vivo imaging with b) activatable FL imaging could delineate the subcutaneous tumors, while c) MR imaging provided enhanced soft-tissue contrast. d) FL and e) MR imaging with T-MAN could also visualize tumors for surgical resection in an orthotopic tumor model. In (d), bioluminescence (BL) from the orthotopic tumor cells confirmed T-MAN uptake in the tumor. In (b) and (c), I–IV represent the activatable, blocking control, nonresponsive control, and activatable and MMP-2 inhibitor groups, respectively. Reproduced with permission.[59] Copyright 2019, American Chemical Society.

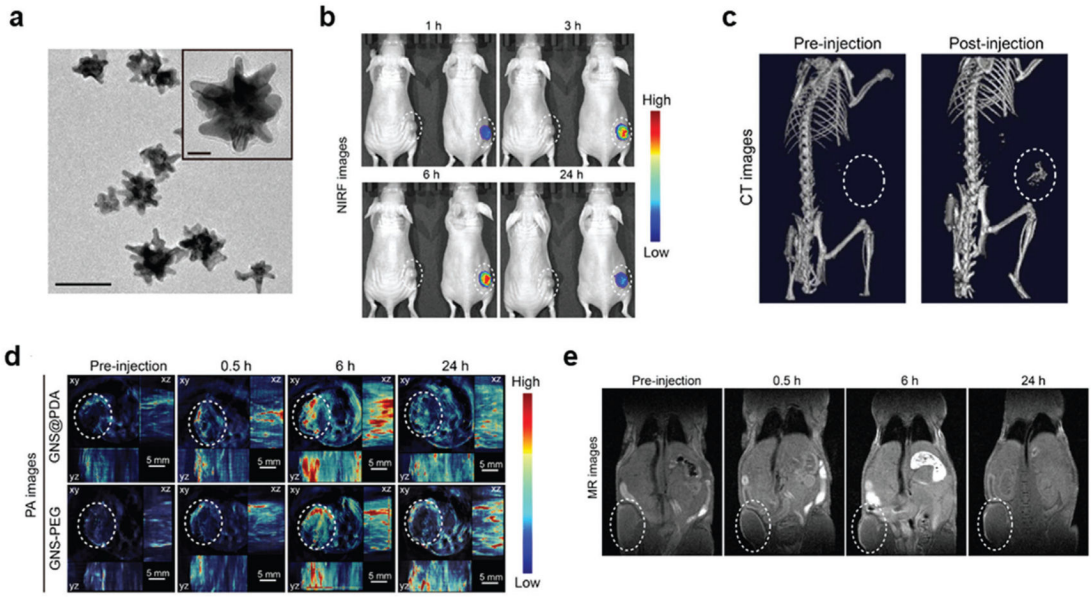

Figure 8.

Serine protease-responsive multimodal imaging. a) TEM image of the synthesized polydopamine-coated gold nanostars (GNS@PDA). Scale bar: 100 μm. b) Activatable NIRF imaging occurred after Cy7-labeled GNS@PDA was cleaved by FAP. Additionally, c) CT, d) PA, and e) MR imaging studies provided high spatial resolution and tissue contrast for tumor delineation. Reproduced with permission.[64] Copyright 2019, American Chemical Society.

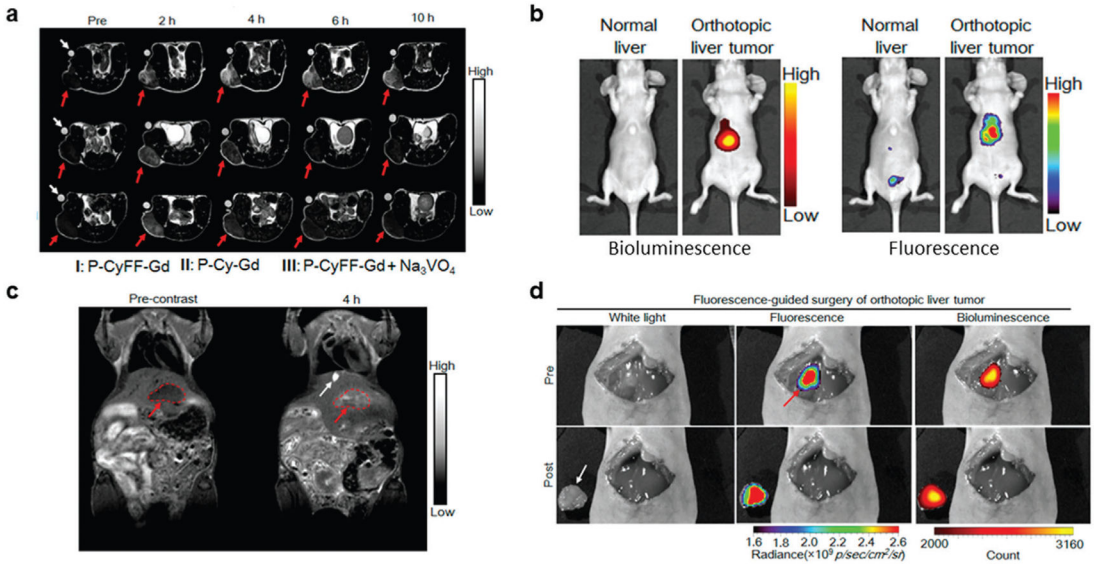

Figure 9.

Other enzyme-responsive multimodal imaging. ALP-specific activation of P-CyFF-Gd resulted in enhanced MR and FL contrast in a) xenograph and b,c) orthotopic tumor models. Imaging in the orthotopic tumor model enabled image-guided surgery to ressect tumor tissue. In (b) and (c), I represents the activatable probe (P-CyFF-Gd), II represents the probe without the ALP substrate (P-Cy-Gd), and III represents the probe and an ALP activity inhibitor (P-CyFF-Gd + Na_3VO_4). Reproduced with permission.[89] Copyright 2019, American Chemical Society.

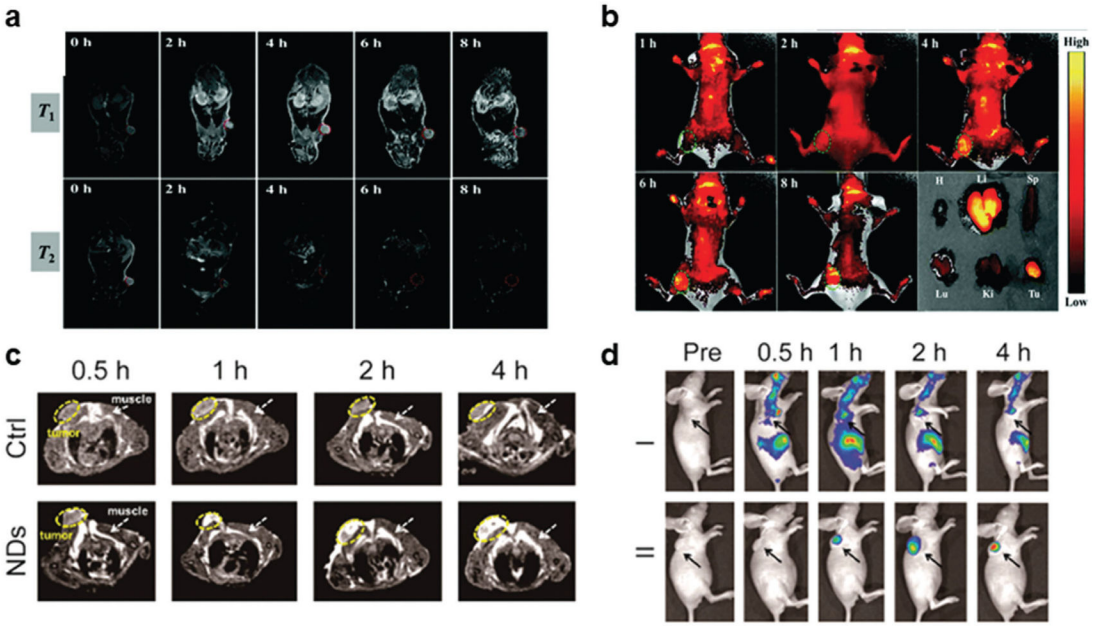

Figure 10.

Multiple stimuli-activated multimodal imaging. FHCPC@MnO_2 nanoflowers were designed to exploit the low pH and high levels of GSH and H_2O_2 that exist in the TME for a) MR and b) FL imaging. A hybrid protein@inorganic nanodumpling (ND) system was designed to be activated by thiols, such as GSH, and low pH. Degradation of the nanosystem in the TME enabled activatable c) MR and d) FL imaging. Reproduced with permission.[86,88] Copyright 2019, RCS Pub and 2020, American Chemical Society.